ASIAN JOURNAL OF CIVIL ENGINEERING (BHRC) VOL. 16, NO. 3 (2015)
PAGES 322-346

INVESTIGATION INTO BEHAVIOR OF CFT CIRCULAR COLUMNS UNDER LONG-TERM AXIAL AND CYCLIC LOADINGS

K. Abedi[1*], A. Nabati[1], H. Afshin[1] and A. Ferdousi[2]
[1]Faculty of Civil Engineering, Sahand University of Technology, Tabriz, Iran
[2]Departement of Civil Engineering,Campuse of Technical and Engineering,Tabriz Branch, Islamic Azad University, Tabriz, Iran

Received: 12 March 2014;**Accepted:** 15 September 2014

ABSTRACT

The objective of this paper is to study the seismic behavior of circular CFT columns under long-term axial loading. Five series of 3-D nonlinear finite element models were developed to investigate the effects of axial load, concrete age, concrete compressive strength, steel tube yield stress and slenderness on one year axial and then cyclic loadings. For creep modeling, RFM method is used to forecast the creep coefficients. Then, the effects of cyclic loading on creeped CFT columns have been investigated. Based on the results, creep causes a reduction in sustainable shear force and ductility ratio and energy absorption capacity of specimens.

Keywords: CFT columns; nonlinear finite element modeling; creep; long-term axial loading; cyclic loading.

1. INTRODUCTION

In recent years, the tendency to build slender structures is increasing but using slender steel or concrete structures solely, has many problems. In steel structures, buckling is an obstacle to be overcome. On the other hand, in concrete structures, the brittle failure is undesired behavior. By combining the mechanical properties of steel and concrete, concrete filled steel tubes (CFT) are a solution to reach to a high strength, ductility and energy absorption capacity. These characteristics are obtained by combining of confinement effect of steel tube which causes the concrete core behaves in a tri-axial stress state and buckling prevention effect of concrete core which prevents steel tube from inward buckling. Beside these advantages, CFT systems suffer from the effects of creep and shrinkage. There are a lot of studies for short-term response of CFT columns but little attention has been devoted to long-term loading response. For the first time, Furlong [1] reported the creep phenomenon in CFT

*E-mail address of the corresponding author: k_abedi@sut.ac.ir (K. Abedi)

columns with a reduction of 15% in load carrying capacity of concrete core after the steel tube began to yield. Terry et al. [2] measured shrinkage and creep strains of CFT columns under axial load for approximately 100 days and concluded that shrinkage of concrete core maybe safely neglected and creep coefficients are 50-60% lower than those in concrete columns. Morino et al. [3] tested 6 axially and 2 eccentrically loaded columns. They showed clear reduction in the creep coefficients of concrete core because of stress redistribution between concrete and steel. Ichinose et al. [4] measured shrinkage and creep strains of two CFT circular columns with different tube thicknesses and one plain concrete column. They reported shrinkage strains are negligible. An experimental study undertaken by Peng [5] showed that creep resulted in an increase in stress of steel tube of 24% after one year loading and an increase of 27% after two years loading. Conversely, stress on the concrete core decreased 47% and 52%, respectively.

Contemporary to experimental studies, a lot of theoretical studies have been carried out to predict the creep behavior of CFT members. This is mainly because the experiments longer than 1 year are rather difficult. Also all the various parameters cannot be investigated in a single experimental program. Thus, analytical tools developed to extrapolate the experimental database to longer time periods and for a larger parametric database.

Wang and Han [6] proposed a model and algorithm for the creep of CFT columns under axial compression load based on the ECPF (Elastic Continuation and Plastic Flow) theory for concrete creep. In the next ten years, based on their proposed model, they developed other predictive models for creep of CFT columns under compressive load with various amount of eccentricities. In these models, multi-axial stresses, effects of steel ratio and strength of concrete on the CFT creep were considered (Wang & Han [7]).By applying a visco-plastic model, namely the Kelvin model, Ichinose [4] predicted the time-dependent behavior of CFT column. Naguib and Mirmiran [8] developed an algorithm by combining the RFM method with double power law function for behavior of CFT with or without the interface bound, Wang et al. [9] developed a model for predicting the creep of high strength CFT columns under axial compression, in which the effects of the concrete mixture on the creep of CFT columns were taken into account. Kwon et al. [10] also carried out an analytical study on the long-term behavior of circular and square CFT columns under axial loading based on the AAEMM, and bound behavior between the concrete core and the steel tube was considered in the studies. Based on their model, Han and Wang [9 and 11] concluded that creep resulted in a decrease in load carrying capacity of approximate 30% for axial compression CFT short columns, and a decrease of 10-30% for the eccentrically loaded members. Also, Han et al. [11] showed that creep reduced the load carrying capacity of CFT members by 10% to 20%. There are a lot of published studies in the seismic behavior of CFT columns; however behavior of concrete-filled unstiffened tubes subjected to repeated cycles of large deformations has received less attention. Prion and Boehme [12] tested three specimens with 152mm outside diameter and 1.65mm steel tube thickness, for high D/t ratios of 92, and concrete cylinder strength of 92MPa. The cyclic tests demonstrated good ductility and energy dissipation of the members. Slight pinching in the hysteretic curves was observed and attributed to the opening and closing of concrete cracks while the steel tube was yielding and buckling. Fracture of the steel tube occurred on the tension side at a strain of approximately three times the yield strain. Boyed et al. [13] tested five circular CFT columns under both constant axial and cyclic loadings. All of the columns had a diameter,

D, of 203.2mm and steel tube thickness, *t*, was either 1.91mm or 2.77mm, for *D/t* ratios of 106 and 73, respectively. Although local buckling occurred in all of the tubes, all columns exhibited stable behavior and maintained the ACI-318-89 predicted load capacity at a minimum displacement ductility, μ, of 6. Alfawakiri [14] tested three hot-formed seamless steel tubes with thickness of 3mm and diameter of 152mm, filled with high strength concrete of 72 or 90MPa. These specimens reached drift in excess of 7%; testing stopped after the specimens exhibited significant local buckling, strength degradation, or fracture on a local buckle. Abedi et al. [21] proposed a novel CFT section which improved the seismic behavior of CFT columns in comparison with current CFT columns.

This paper outlines investigation into the effects of creep phenomenon of CFT circular columns on stress variations of steel and concrete by using RFM method for predicting the creep coefficients. Also a comparison of seismic response of CFT columns under short-term axial loading with CFT columns under long-term axial loading has been carried out. Axial load and lateral displacements are applied at the top of columns to simulate the constant dead load and seismic loading, respectively. Also, the effects of creep on the reduction of ductility ratio and energy absorption capacity of CFT specimens are presented. Furthermore, creep modeling and all of the analyses have been undertaken using ANSYS12.0 [15] and ANSYS CIVIL FEM12.0 [16], which is designed specifically for advanced structural analysis. Therefore, the aims of this study are as follows:

- Finite element modeling of creep in CFT columns,
- Study on the variations of stresses in concrete and steel,
- Comparison of behavior of CFT columns under long-term axial and cyclic loads with CFT columns under short-term axial and cyclic loads

2. CREEP

Creep is an under load time-dependent deformation, while shrinkage is an unloaded time-dependent deformation. Because the modulus of elasticity of concrete increases with age, the elastic deformation gradually decreases (Fig. 1). Time-dependent deformation of a concrete member under constant stress (Fig. 1) is computed as mentioned in equation (1):

$$\varepsilon_t(t) = \varepsilon_{el} + \varepsilon_{cr}(t) + \varepsilon_{sh}(t) \quad (1)$$

where ε_{el} is instant elastic strain, $\varepsilon_{cr}(t)$ is creep strain at age t and $\varepsilon_{sh}(t)$ is shrinkage strain at age t. According to the experimental results (Terry et al. [2] & Ichinose et al. [4]), the shrinkage of the concrete core of CFT columns is negligible. Therefore, in this study the effects of shrinkage of CFT columns are not considered.

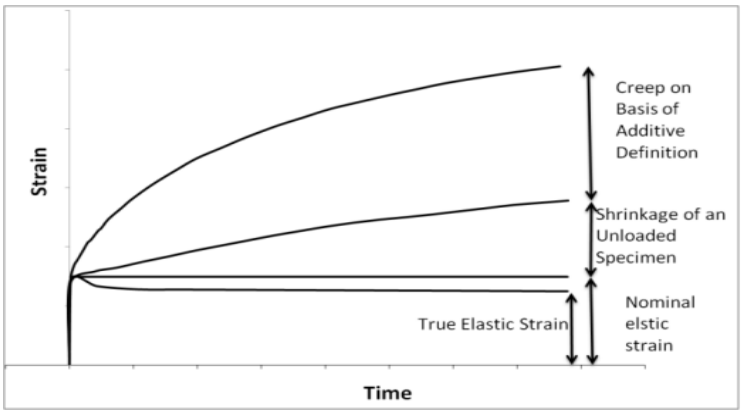

Figure 1. Change in strain of loaded and drying specimen

2.1 Creep effects on CFT columns

There are some creep models for evaluating the creep of concrete core of CFT columns such as Effective Modulus Method (EMM), Age Adjusted Effective Modulus Method (AAEMM), Rate of Creep Method (RCM), and Rate of Flow Method (RFM) which are linearized creep laws and ACI 209R-92, CEB MC90, GL2000, and B3. In the present study, the RFM method is used because of its simplicity and accuracy. This method approximates the creep coefficients and strains by combining the EMM and RCM methods.

During creep phenomenon in CFT columns, deformation will increase, and stresses on cross-section and internal forces in the columns will redistribute. In other words, the concrete core will be in the situation of unloading, meanwhile, the steel tube will bearing more stresses. In general, creep will raise stresses on the steel tube about 5-27% and decrease those on the concrete core about 20-52% (Wang et al. [17]).

3. FINITE ELEMENT MODELING OF CFT COLUMNS

In order to demonstrate the differences between behavior of CFT columns under short-term axial and then under cyclic loading and CFT columns under long-term axial and then under cyclic loading, nonlinear geometric and material finite element analyses have been carried out.

There are two hypotheses about creep which are intended in FEM analysis. One of the hypotheses is linearity, means that strain is proportional to stress as mentioned in equation (2):

$$\varepsilon(t,\tau) = \sigma_c(\tau).\left[\frac{1}{E_c(\tau)} + \frac{\varphi(t,\tau)}{E_{c,28}}\right] = \sigma_c(\tau).\Phi(t,\tau) \tag{2}$$

where $\sigma_c(\tau)$ is constant stress applied at time τ, $E_{c,28}$ is elasticity modulus at 28 days, $E_c(\tau)$ is elasticity modulus at loading age τ, $\varphi(t,\tau)$ is creep coefficient and $\Phi(t,\tau)$ is creep function. Validity of linearity hypothesis is experimentally confirmed for initial stresses not greater than 40% of concrete mean compressive strength.

Another hypothesis commonly accepted is the superposition principle, which implies that the strain produced in concrete at any time t by any increase of stress applied in time τ, is independent from any increase of stress produced before or after τ. Creep strains are, therefore, addable. So the total strain of concrete for a history of variable loads should be as equation (3):

$$\varepsilon_{tot}(t) = \varepsilon_{sh}(t) + \int_{\tau=0}^{\tau=t} \Phi(t,\tau).d\sigma(\tau) \tag{3}$$

where $\varepsilon_{tot}(t) is$total strain at time t, $\varepsilon_{sh}(t)$ is shrinkage strain at time t, $\Phi(t,\tau)$ is creep function and $d\sigma(\tau)$ is stress variation at time τ. For the calculation of the integral of equation, the step by step standard method is used. In the step by step method, the time is divided into a series of intervals, so that in each of the intervals, the equilibrium and compatibility conditions of the structure are satisfied. To do so, time t is divided into times series t_0, t_1,t_2, ..., t_k. Strain is computed as mentioned in equation (4):

$$\varepsilon(t_k) = \sum_{i=1}^{k}\left[\frac{1}{E_c(t_i)} + \frac{\varphi(t_k,t_i)}{E_{c,28}}\right].\Delta\sigma(t_i) = \sum_{i=1}^{k}\Phi(t_k,t_i).\Delta\sigma(t_i) \tag{4}$$

The solution procedure employs a nonlinear calculation with automatic time discretization: the time steps, corresponding to “load steps” and “sub steps”, are chosen to follow the evolution of loads and model geometry. Strain increments produced by creep are computed from creep coefficients defined in the material and from stress increments produced during time discretization as mentioned in equation (5):

$$\Delta\varepsilon_{cr}(t_k) = \varepsilon_{cr}(t_k) - \varepsilon_{cr}(t_{k-1}) = \sum_{i=1}^{k}\frac{\varphi(t_k,t_i)}{E_{c,28}}.\Delta\sigma(t_i) - \varepsilon_{cr}(t_{k-1}) \tag{5}$$

These creep strains are introduced in the model using User Programmable Feature of ANSYS. Also computed creep coefficients using RFM method are considered to calculations at every step.

3.1 Elements characteristics

Three types of elements are used in modeling of CFT columns. These elements are Solid 65 for modeling concrete core, Solid 45 for modeling steel tube, and Contact 52 which is used to model contact between concrete core and steel tube. The element of Solid 65 is defined by eight nodes having three translational degrees of freedom at each node. This solid element is capable of cracking in tension and crushing in compression, plastic deformation and creep. The criterion for failure of concrete due to a multi-axial stress can is expressed in equation (6):

$$\frac{F}{f_c'} - S \geq 0 \tag{6}$$

where F is a function of the principal stress state σ, S is the failure surface expressed in terms of principle stresses and five input parameters f_t , $f_c^{'}$, f_{cb} , $f_1 and f_2$ (f_t:ultimate uniaxial tensile strength, $f_c^{'}$ ultimate uniaxialcompressive strength, f_{cb}: ultimate biaxialcompressive strength, f_1: ultimate compressive strength for a state of biaxial compression superimposed on hydrostatic stress state, f_2: ultimatecompressive strength for a state of uniaxial compression superimposed on hydrostatic stress state). Fig. 2 shows the failure surface in principal stress space σ_{zp} close to zero.

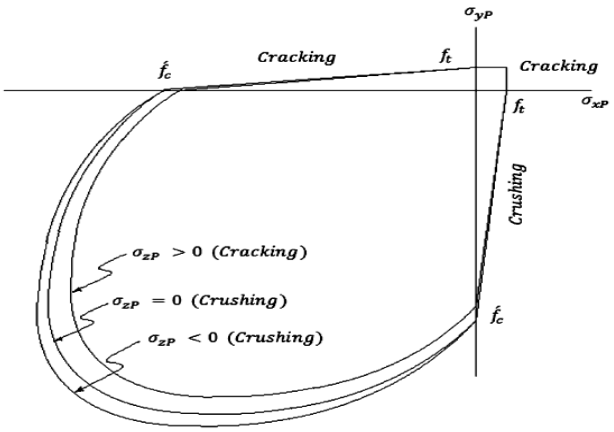

Figure 2. Failure surface in principal stress space $\boldsymbol{\sigma_{zp}}$ close to zero

A three-dimensional solid element (SOLID 45) has been used to model the steel tube. This element has good compatibility with isoparametric solid element of concrete core. The element has plasticity, stress stiffening, large deflection and large strain capabilities. Three dimensional node to node contact elements (Contact 52) have been used to model the contact between steel tube and concrete core. The element is located between two adjacent nodes of steel tube and concrete core and is capable of modeling the separation, sliding and contact between two nodes during the loading process. The element is capable of supporting only compression in the direction normal to the surface and shear in the tangential direction (Coulomb friction). This element has three translational degrees of freedom at each node. Also, it may be initially preloaded in the normal direction or it may be given a gap specification. A specified stiffness acts in the normal and tangential direction when the gap is closed and not sliding. The assumptions of this element are friction coefficient (μ), stiffness in the normal direction (K_N), stiffness in the tangential direction (K_S), initial penetration and initial conditions of gap (closed or open). Figs. 3 and 4 show three-dimensional node to node contact element (Contac 52) and its force-deflection relationship, respectively.

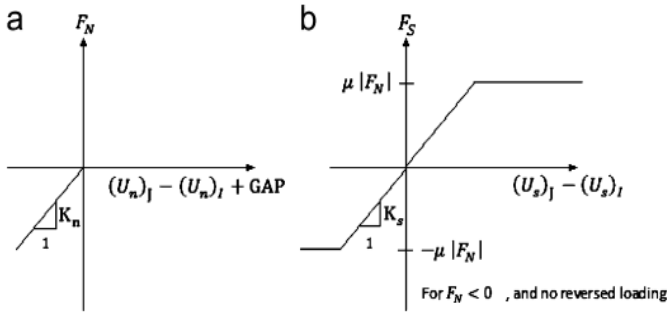

Figure 3. Force-deflection relationship for contact element used to model the contact between steel tube and concrete core

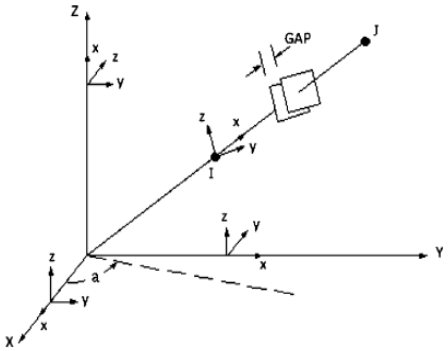

Figure 4. Three-dimensional node to node contact elements (Contact 52)

3.2 Material characteristics

The stress-strain behavior of concrete core and steel tube which are used in analyses, are shown in Fig. 5 and 6, respectively. One of the important issues in creep analysis is the Poisson's ratio selection. There are three kinds of Poisson's ratios: the static or short-term Poisson's ratio ($\nu_s = \frac{lateralelasticstrains}{axialelasticstrains}$), the creep Poisson's ratio ($\nu_c = \frac{late\ ralnetcreepstrains}{axialnetcreepstrains}$) and effective Poisson's ratio ($\nu_{Effective} = \frac{totalelasticstrain}{totalelasticstrain}$). Gopalkrishnan et al. [18] showed that the effective Poisson's ratio is constant with time for multi- axial state of stress. Later, Jordan and Illston [19] concluded that the creep Poisson's ratio and the effective Poisson's ratio remain approximately constant with time and equal to the static or elastic value as long as the load is sustained. So in the entire analysis Poisson's ratio is selected as constant elastic one.

3.3 Verification of finite element modeling

In order to validate the accuracy of models, a comparison between numerical results of finite element modeling and experimental results of CFT columns under long-term axial and cyclic loading have been carried out. Regarding long-term axial loading, two specimens have been selected with specification according to the table 1. UCFT refers to specimen in which there is no bound between steel and concrete and reversely, BCFT refers to specimen with full bond between steel and concrete. For UCFT specimen, axial load is applied to

concrete core and for BCFT specimen, axial load has been applied to the both concrete core and steel tube.

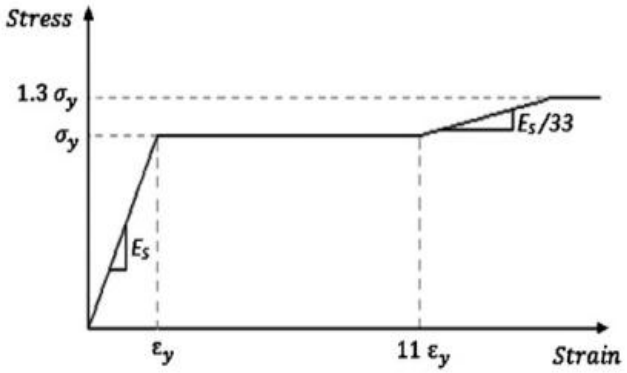

Figure 3. The stress-strain relationship for steel tube

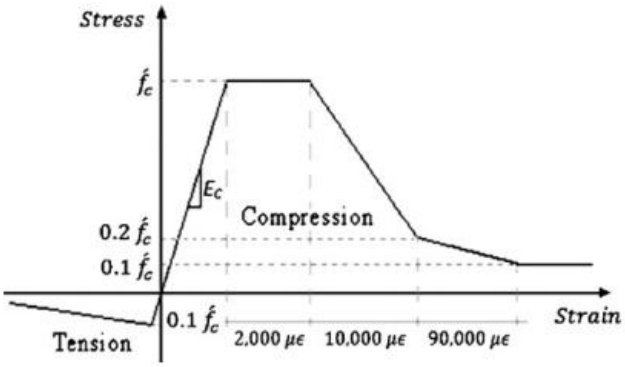

Figure 4. The stress-strain relationship for concrete

Table 1: The specifications of the experimental creep model according to Terry [2]

Specimen	Concrete age at loading (days)	Creep parameter	Sustained load(KN)	Concrete compressive strength(Mpa)	Tube thickness (mm)	Inside diameter (mm)	Height(mm)
UCFT	18	0.147	350	45.2	1	196mm	600mm
BCFT	18	0.147	351	45.2	1.5	196mm	600mm

Figs. 7 & 8 show experimental and numerical axial strain-time responses under axial loading for approximately 100 days for UCFT and BCFT specimens, respectively (Naguib & Mirmiran model and finite element modeling). Fig. 9 illustrates creep mechanism in UCFT and BCFT columns. It can be seen from Fig. 10 that analytical results are close to the experimental ones. In Fig. 11, analytical curve is closer to experimental curve in comparison with numerical results achieved by Naguib [8]. This is mostly related to the selection of creep coefficients. For UCFT and BCFT specimen creep coefficients of ACI φ=1.2 and φ=1.0 are used, respectively.

Regarding cyclic loading, another model has been analyzed. For this purpose, a CFT

column according to the Table 2 has been selected. Fig. 12 shows the loading condition for c21c20 specimen. According to Fig. 13, the cyclic response of the finite element model is close to that of experimental one. Therefore, it has been found that the finite element model is reliable enough to be used to undertake creep analyses for CFT members.

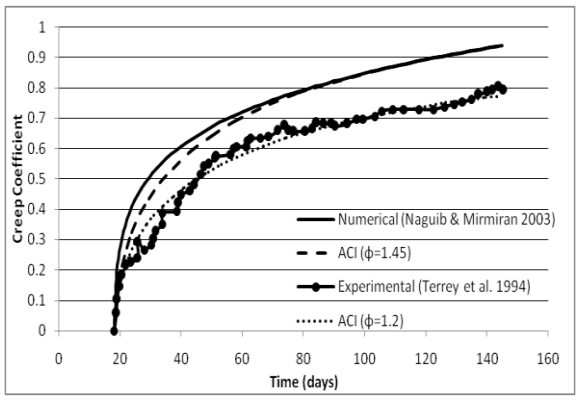

Figure 5. Creep coefficients for UCFT specimen

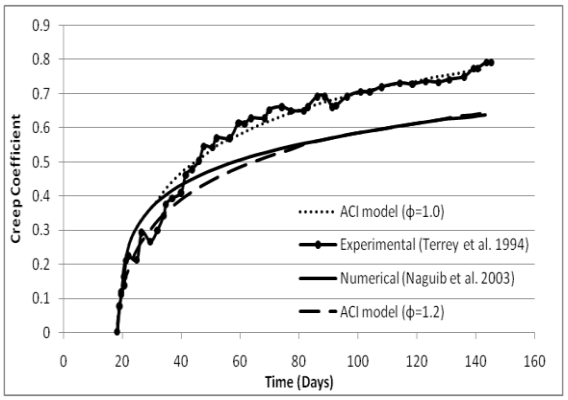

Figure 6. Creep coefficients for BCFT specimen

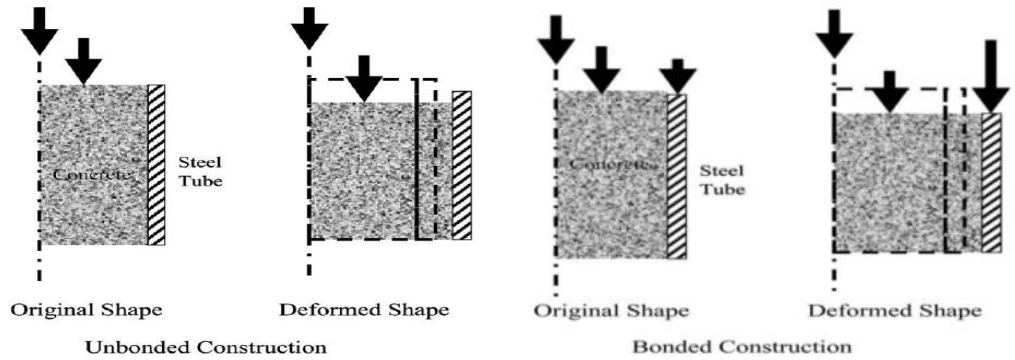

Figure 7. Creep mechanism in UCFT and BCFT columns

Table 2: The specifications of the cyclic loading experimental model according to Choi [20]

Specimen	t(mm)	D/t	$f_c^{'}$(Mpa)	N_0(KN)	N/N_0	Yield stress(Mpa)	Tensile strength(Mpa)
C21c20	6.6	21.2	36.8	1420	0.2	295	352

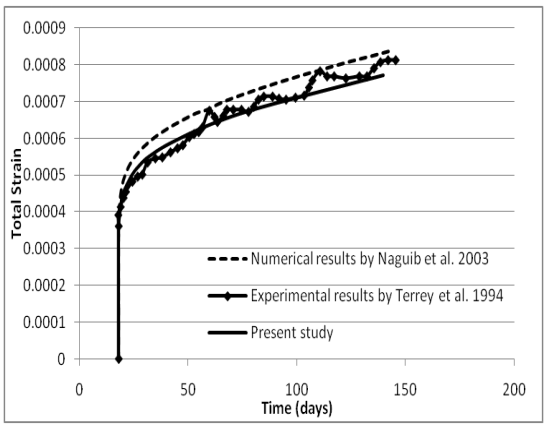

Figure 8. Creep strains for UCFT specimen

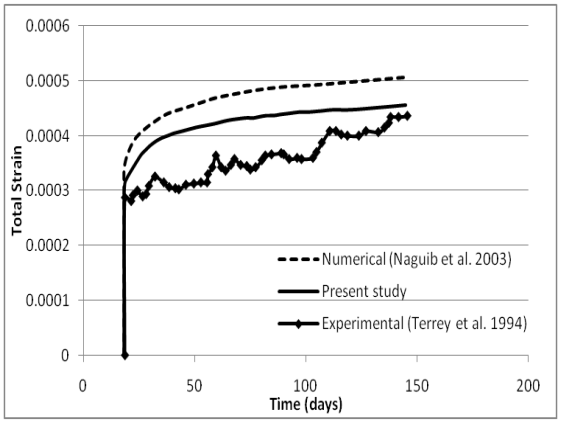

Figure 9. Creep strains for BCFT specimen

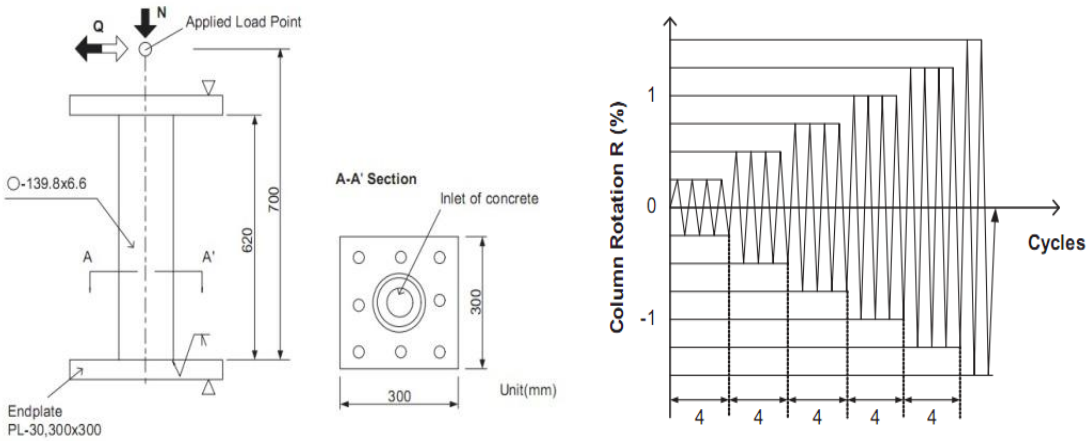

Figure 10. Loading condition for circular CFT column specimen for cyclic test ($N_0 = 0.89A_s f_{sy} + A_c(0.85f_c^{'} + 0.78\frac{2t}{D-2t}f_{sy})$

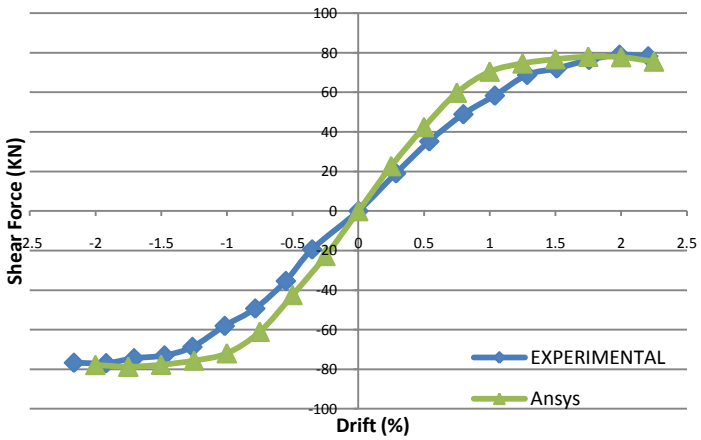

Figure 11. The experimental and numerical shear force- drift enveloping curves of C21C20 specimen under axial and lateral cyclic loading

4. NUMERICAL RESULTS

To investigate into the effects of various parameters, 5 series of CFT columns have been considered for analyses. The specimens are named from A to E. In all groups, most of the parameters are constant except one parameter and the influence of variable parameter is investigated on the creep behavior of CFT columns under axial and cyclic loading. Since application of CFT is mostly in high-rise buildings and bridge pier columns, sustained loads may be as high as 35% of column load carrying capacity. Therefore in group A, the proportion of axial load to axial bearing capacity is selected 0.2, 0.3 and 0.4. In group B, the variable parameter is concrete age, which differs from 7 to 90 days. Results of group C, demonstrate the influence of concrete compressive strength on creep phenomenon and hysteresis behavior. Tube yield stress influence is studied in group D, considering yield stresses of 295, 395, and 495 MPa. Finally the effect of slenderness of CFT column will be investigated in group E. In other words, the *L/D* proportions (column length/outside diameter) are 3, 5, and 8. Table 3 shows the specifications of numerical models. All the columns are considered as fixed-end columns. Furthermore, all of the finite element analyses are carried out in two consecutive phases: creep analysis and then seismic analysis. At first, creep analyses begin with long-term axial loading. In this phase, average creep coefficients of UCFT and BCFT of RFM method are used. This is mainly because bound between concrete core and steel tube in reality is not completely unbounded or completely bounded. Also a comparison with ACI coefficients is shown for every curve.As mentioned before, in the process of creep phenomena, the concrete core will be in the situation of unloading (stress reduction), whereas, the steel tube will bear more stresses (stress increase). In general, creep will increase stresses on the steel tube and decrease those on the concrete core.

$$R = \frac{\delta}{L} = 1\,,2\,,3\,,4\,\% \tag{7}$$

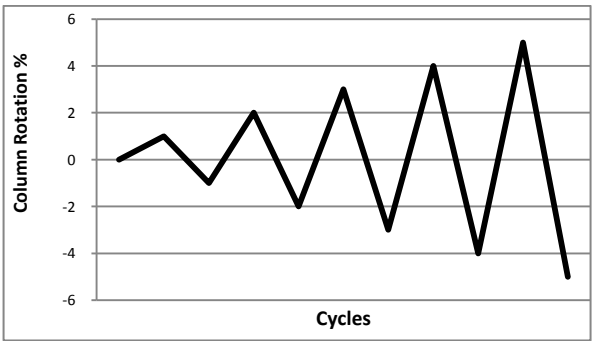

Figure 12. Number of cycles-lateral displacement history

In second phase, after long-term axial loading, cyclic lateral displacements are applied according to the Fig. 14 and Eq. 7. Then, for the purpose of comparison, the same models are analyzed under cyclic loading with short-term axial loads.

4.1 Numerical results of the cft specimens under long-term axial loading (creep analyses)

For every group, creep coefficients, the variation of total strains for each model under long-

term load and the variation of Von-Mises stress have been shown. As the age of concrete increases, compressive strength and elasticity modulus of concrete will increase. As a sample, Table 4 shows these variations gained from ACI specifications for specimens of group A.

Table 3: The specifications of models

Specimen	Constant Parameters							Variable Parameters	
	Length (mm)	Yield stress (Mpa)	Concrete Compresive Strength (Mpa)	Tube Thickness (mm)	Outside Diameter (mm)	Axial Load/ Axial Capacity	Concrete Age (days)	Axial Load/ Axial Capacity	
A-N-2	3000	295	30	18	580		28	0.2	
A-N-3	3000	295	30	18	580		28	0.3	
A-N-4	3000	295	30	18	580		28	0.4	
								Concrete age (days)	Concrete Compressive Strength (MPa)
B-t-7	3000	295		18	580	0.3		7	21.106
B-t-28	3000	295		18	580	0.3		28	30
B-t-60	3000	295		18	580	0.3		60	32.72
B-t-90	3000	295		18	580	0.3		90	33.54
								Concrete Compressive Strength (Mpa)	
C-f-20	3000	295		18	580	0.3	28	20	
C-f-30	3000	295		18	580	0.3	28	30	
C-f-40	3000	295		18	580	0.3	28	40	
								Yield Stress (Mpa)	
D-f_y-2	3000		30	18	580	0.3	28	295	
D-f_y-3	3000		30	18	580	0.3	28	395	
D-f_y-4	3000		30	18	580	0.3	28	495	
								L/D	Outside Diameter (mm)
E-S-3		295	30	18	580	0.3	28	3	1740
E-S-5		295	30	18	580	0.3	28	5	3000
E-S-8		295	30	18	580	0.3	28	8	4640

Table 4: Variation of concrete specifications

concrete age(days)	compressive strength(Mpa)	modulus of elasticity(Pa)
28	30	2.93E+10
393	34.887	3.16E+10

- GROUP A

In this group, the amount of axial load is variable parameter. Fig. 15 shows the creep coefficients of numerical models, their average and the nearest ACI coefficients. Fig. 16 shows that total strain of A-N-4 specimen is more than that of the other specimens. This is mainly due to higher axial load of A-N-4 specimen. Because in CFT columns, the regions near the supports are critical, so the nodes inside that region are selected. Fig. 17 shows the steel and concrete nodes which are selected to gain Von-Mises stress variation. Fig. 18 shows the finite element mesh of CFT columns. Fig. 19 and 20 show variation of Von-Mises stress in concrete and steel nodes, respectively.

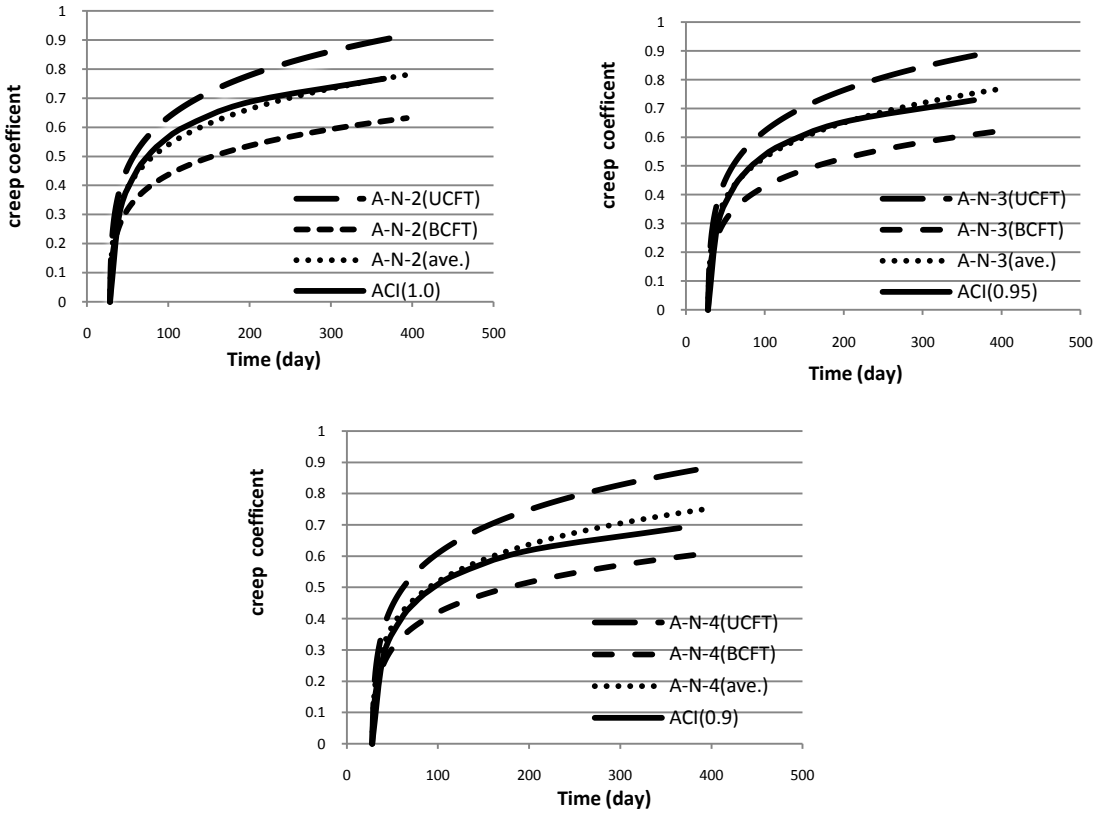

Figure 13. Creep coefficients of group A

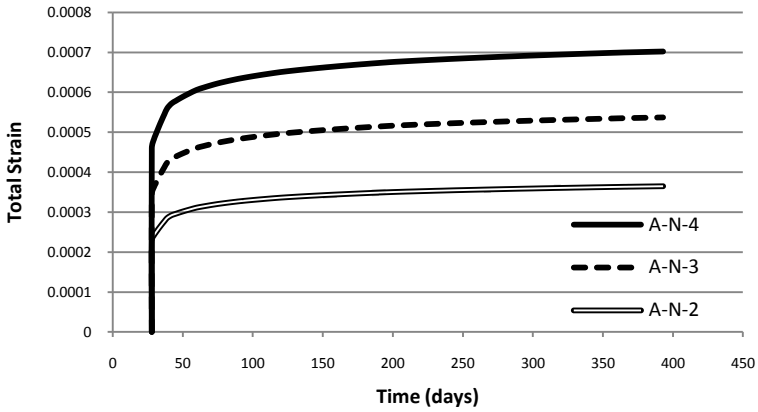

Figure 14. Total strain-time curve

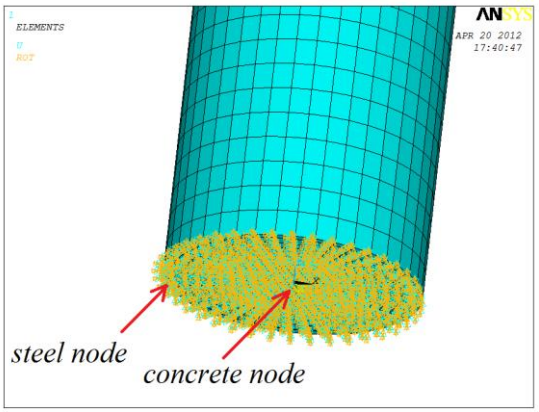

Figure 15. Selected steel and concrete nodes

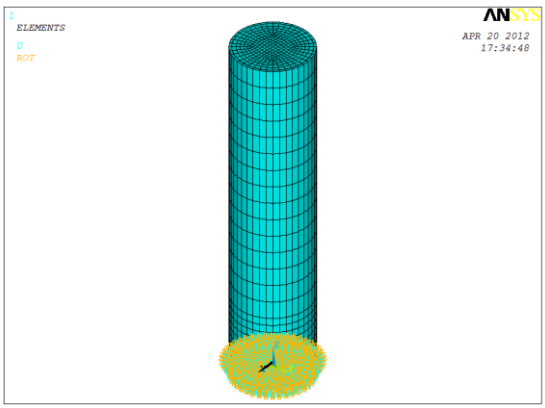

Figure 16. Finite element mesh

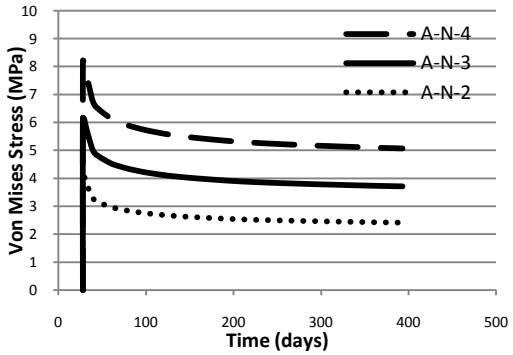

Figure 17. Variation of Von-Mises stress in concrete node

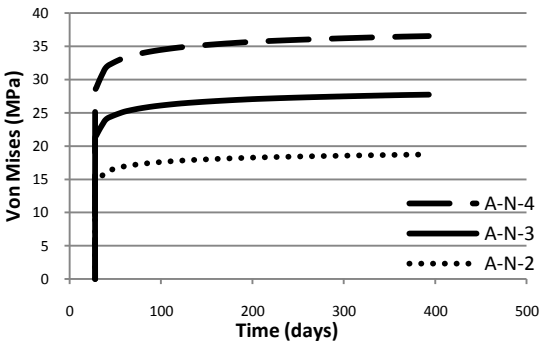

Figure 18. Variation of Von-Mises stress in steel node

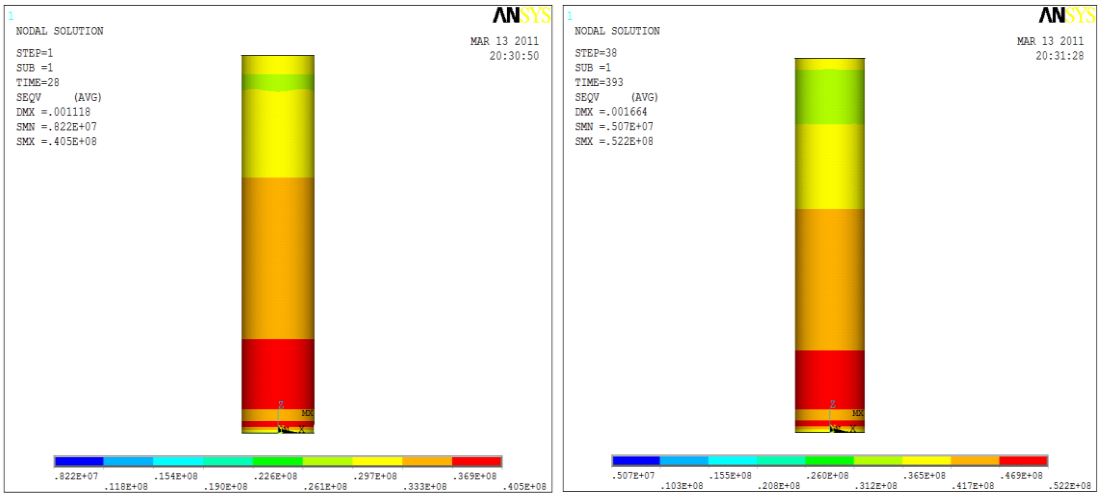

Figure 19. Von-Mises stress contours of steel in days 28 and 393 for A-N-4 specimen

Fig. 19 shows during the long-term axial load, the Von-Mises stresses on a selected concrete node decrease. These decreases for specimens A-N-2, A-N-3, A-N-4 are 41.36%, 39.77%, 38.25%, respectively.

Conversely, Fig. 20 shows that in steel nodes, during long-term load, Von-Mises stresses increase in specimens A-N-2, A-N-3, A-N-4, 32.27%, 30.7%, 29.1%, respectively. Fig. 21 shows the increase in steel stress and Fig. 22 shows the decrease in concrete stress using Von-Mises contours after one year loading.

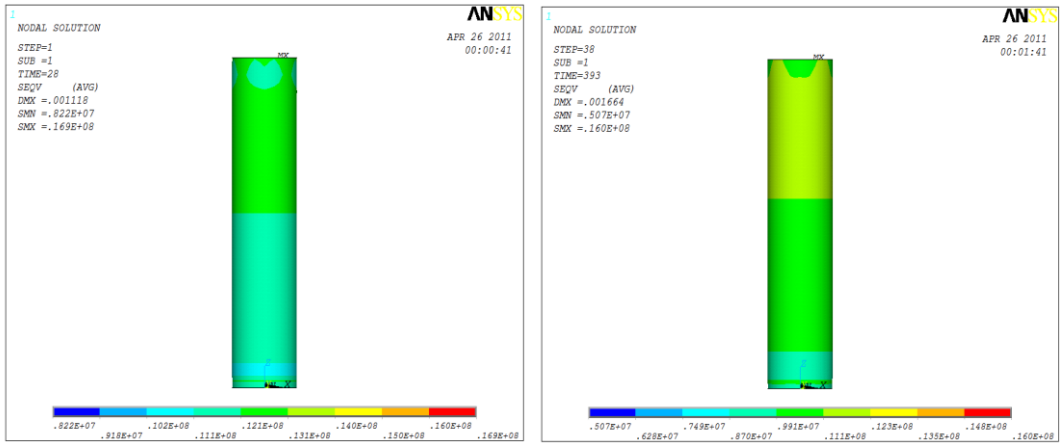

Figure 20. Von-Mises stress contours of concrete in days 28 and 393 for A-N-4 specimen

- GROUP B

In this group, the age of concrete is variable parameter. Calculated creep coefficients using RFM method for B-t-7, B-t-28, B-t-60 and B-t-90 specimens are near to 1.0, 0.95, 0.9, and 0.85, respectively (according to ACI specifications). Fig. 23 shows that total strain of B-t-7 specimen is more than that of the other specimens. This is mainly due to lower concrete age and modulus of elasticity which result in higher total strains.

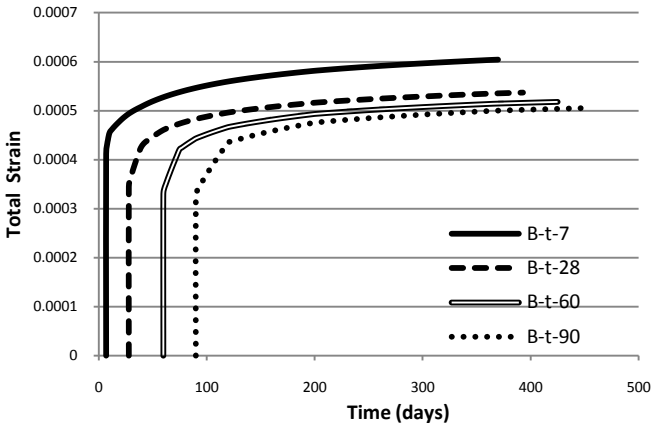

Figure 21. Total strain-time curve for group B

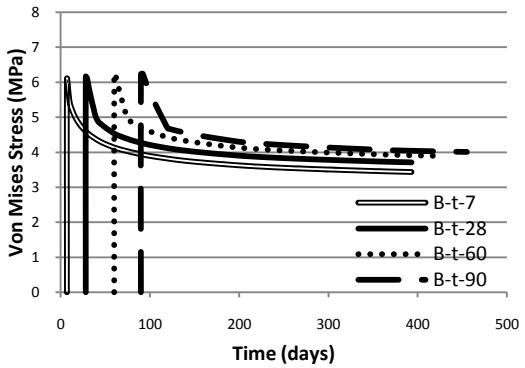

Figure 22. Variation of Von-Mises stress in concrete node

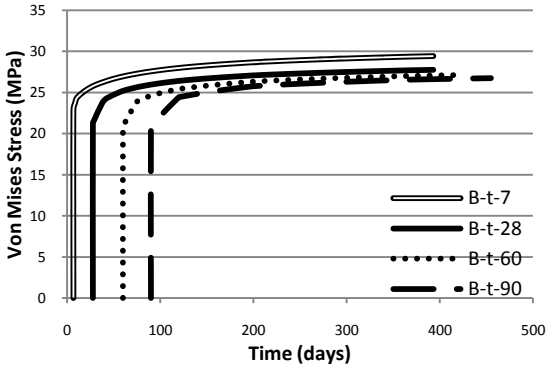

Figure 23. Variation of Von-Mises stress in steel node

Figs. 24 and 25 show variation of Von-Mises stress at selected nodes in concrete and steel, respectively. Fig. 24 shows during the long-term axial load, Von-Mises stress on a selected concrete node decreases. These decreases for specimens B-t-7, B-t-28, B-t-60 and B-t-90 are 43.58%, 39.77%, 37.25% and 35.7%, respectively. Conversely, Fig. 25 shows during long-term load, in steel nodes, Von-Mises stresses increase in specimen B-t-7, B-t-28, B-t-60 and B-t-90, 28%, 31%, 30.23% and 28.94%, respectively.

- GROUP C

In this group, the amount of compressive strength of concrete is variable parameter. Calculated creep coefficients by using RFM method for C-F-20, C-F-30, and C-F-40 specimens are near to 0.95, 0.95, and 0.97, respectively (according to ACI specifications). Also, the applied axial load of every column is 0.3 of column axial load capacity. So the applied axial load of C-F-40 specimen and the total axial strain are higher than those of others (Fig. 26). Figs. 27 and 28 show variation of Von-Mises stresses at selected nodes in concrete and steel, respectively. Fig. 27 shows during the long-term axial load, Von-Mises stress on a selected concrete node decreases. These decreases for specimen C-F-20, C-F-30, C-F-40 are 37.75%, 39.77%, 39.4%, respectively. Conversely, Fig. 28 shows during long-

term load, in steel nodes, Von-Mises stresses increase in specimen C-F-20, C-F-30, and C-F-40, 29.7%, 31%, and 30.45%, respectively.

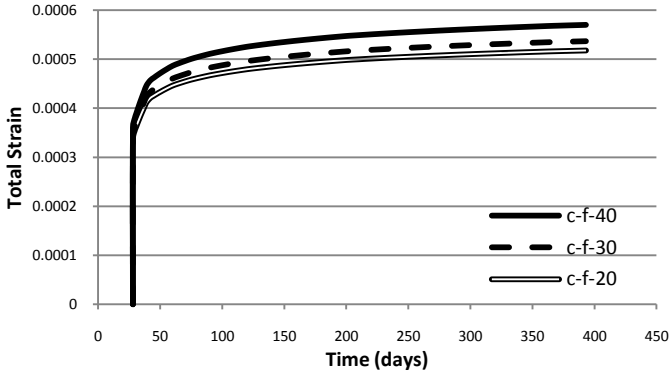

Figure 24. Total strain-time curve for group C

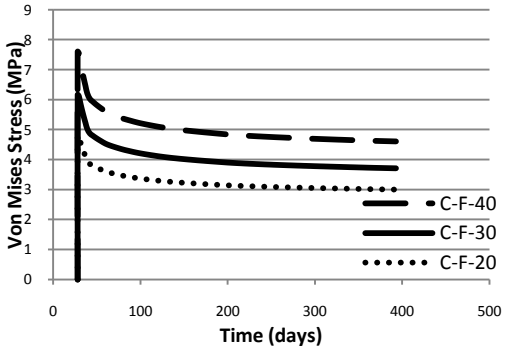

Figure 25. Variation of Von-Mises stress in concrete node

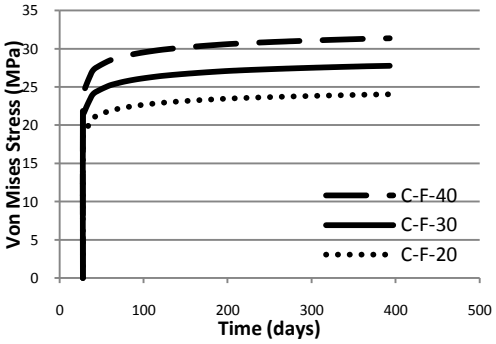

Figure 26. Variation of Von-Mises stress in steel node

- GROUP D

In this group, the amount of yield stress of steel tube is variable parameter. Calculated creep coefficients using RFM method for D-fy-2, D-fy-3, and D-fy-4 specimens are near to 0.95, 0.95, and 0.97, respectively (according to ACI specifications).

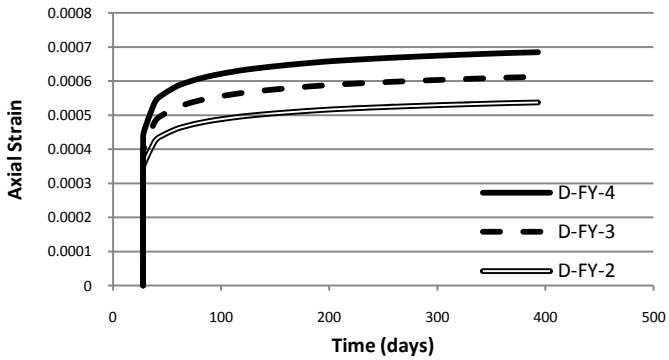

Figure 27. Total strain-time curve for group D

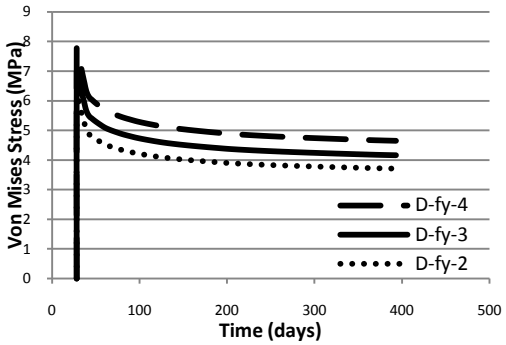

Figure 28. Variation of Von-Mises stress in concrete node

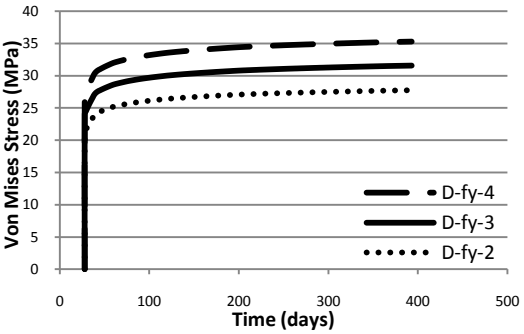

Figure 29. Variation of Von-Mises stress in steel node

In this group, the applied axial load of every column is 0.3 of column axial load capacity. So the applied axial load of D-fy-4 specimen and the total axial strain are higher than those of the others (Fig. 29). Figs. 30 and 31 show variation of Von-Mises stress at selected nodes in concrete and steel, respectively. Fig. 30 shows, during the long-term axial load, Von-Mises stress on a selected concrete node decreases. These decreases for specimen D-fy-2, D-fy-3, and D-fy-4 are 39.77%, 40.4%, and 40.3%, respectively. Conversely, Fig. 31 shows, during long-term load, in steel nodes, Von-Mises stress increase in specimen D-fy-2, D-fy-3, and D-fy-4, 30.66%, 31.5%, and 31.31%, respectively.

- GROUP E

In this group, the value of slenderness of column is variable parameter. According to RFM method, for creep coefficients, column length has no effect on the value of coefficients. So for group E, one curve of creep coefficients exists and the amount of creep coefficients are near to 0.95(according to ACI specifications showed in fig. 32).

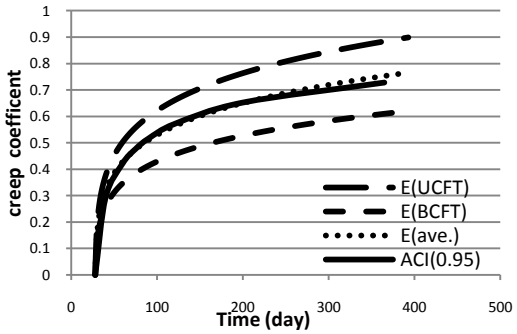

Figure 30. Creep coefficients of group E models

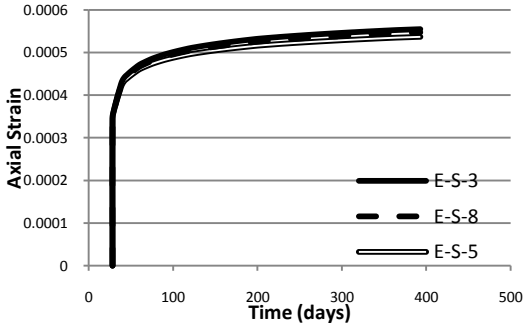

Figure 31. Total strain-time curve for group E

In this group, the applied axial load of every column is 0.3 of column axial capacity. So the total axial strain for all of the specimens are almost equal (Fig. 33). Figs. 34 and 35 show variation of Von-Mises stresses at selected nodes in concrete and steel, respectively.

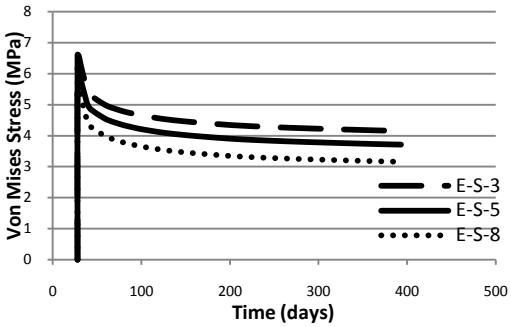

Figure 32. Variation of Von-Mises stress in concrete node

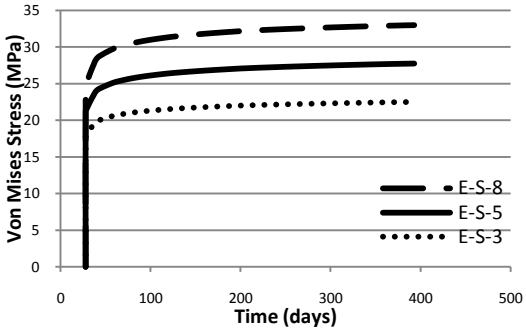

Figure 33. Variation of Von-Mises stress in steel node

Fig. 34 shows during the long-term axial load, the Von-Mises stress on a selected concrete node decreases.These decreases for specimen E-S-3, E-S-5, E-S-8 are 37.16%, 39.77%, 44.56%, respectively. Conversely, Fig. 35 shows in steel nodes, during long-term load, Von-Mises stresses increase in specimen E-S-3, E-S-5, and E-S-8, 25.83%, 30.72%, and 33.76%, respectively.

4.2 Numerical results of the CFT specimens under long-term axial and lateral cyclic loading

In this section, the influence of long-term axial loading on seismic behavior of CFT columns is investigated by comparing with the behavior of the same samples under short-term loading. Therefore, for all the creeped specimens, by maintaining of the stress variations and long-term load which is equal to short-term one, lateral displacements are applied according to Fig. 14.

- GROUP A

Fig. 36 shows the hysteretic curves for CFT columns of group A. According to table 5, by increasing the axial load, reduction percentage of sustainable shear force increases in the same drifts.

Table 5: Reduction percentages of sustainable shear force for specimens of group A

Specimen	**Drift**		
	1%	2%	3%
A-N-2	1.37	1.5	3.1
A-N-3	1.59	2.31	5.3
A-N-4	2.87	4.15	--------

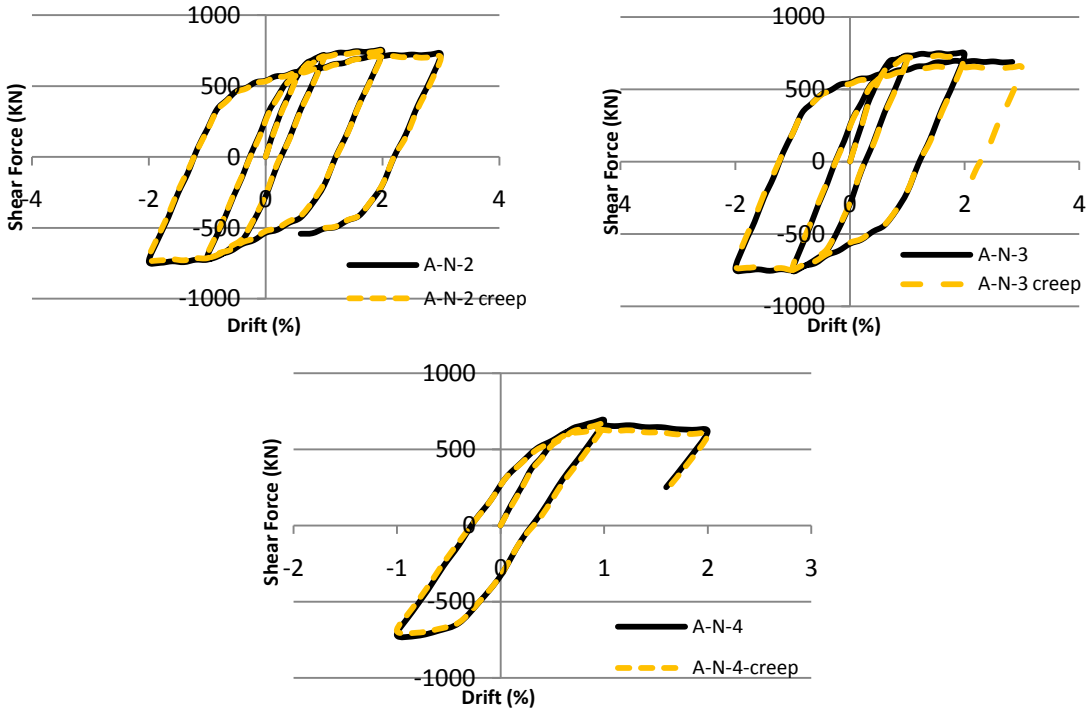

Figure 34. Hysteretic curves for CFT columns of group A

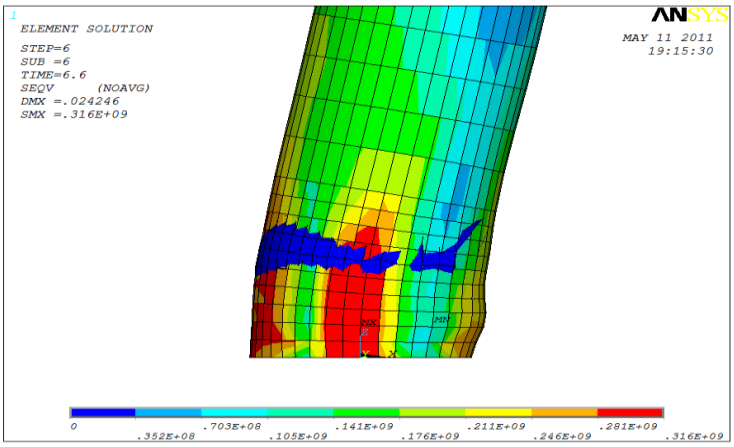

Figure 35. Local buckling of A-N-4 specimen

Creep causes a reduction in ductility ratio $\left(\mu' = \frac{displacment\ \ of\ 95\%\max\ \ sustainable\ \ shear\ force}{displacment\ \ of\ first\ yielding\ \ or\ local\ buckling\ \ of\ steel}\right)$ of specimens. The reductions of ductility ratio for specimens A-N-2, A-N-3, A-N-4 are 15, 7, and 1%, respectively. By inspecting the hysteretic curves, as an average amount, creep causes a reduction of 2% in energy absorption capacity of CFT columns. Fig. 37 shows the buckled A-N-4 specimen at the end of the analysis.

- GROUP B

Fig. 38 shows the hysteretic curves for CFT columns of group B. In this group, the hysteretic curves are very close to each other. This is mainly due to almost equal concrete specifications after one year of loading.

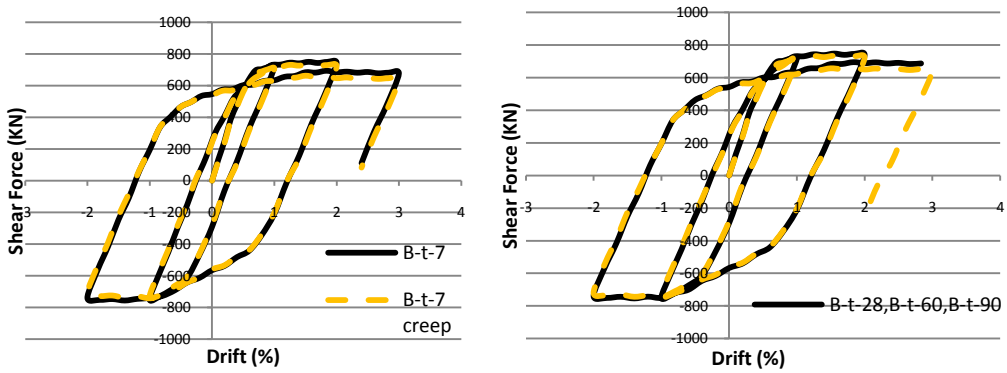

Figure 36. Hysteretic curves for CFT columns of group B

According to Table 6, by increasing the concrete age, reduction percentages of sustainable shear force decrease in the same drifts. Creep causes a reduction in ductility ratio of specimens. These decreases for specimens B-t-7, B-t-28, B-t-60 and B-t-90 are 4.2%, 6.7%, 6.7%, and 6.7%, respectively. Also as an average amount, creep causes a reduction of 2% in energy absorption capacity of CFT columns.

Table 6: Reduction percentages of sustainable shear force for specimens of group B according to Fig. 38

Specimen	**Drift**		
	1%	2%	3%
B-t-7	1.73	2.77	5.38
B-t-28, B-t-60, B-t-90	1.59	2.31	5.3

- GROUP C

According to Table 7, by increasing the compressive strength, reduction percentages of sustainable shear force increase in the same drifts. Creep causes a reduction in ductility ratio of specimens. These decreases for specimens C-F-20, C-F-30 are 11.7%, 13%, respectively. Also as an average amount, creep causes a reduction of 1.74% in energy absorption capacity of CFT columns.

Table 7: Reduction percentages of sustainable shear force for specimens of group C according to Fig. 39

Specimen	**Drift**		
	1%	2%	3%
C-F-20	0.9	1.77	2
C-F-30	1.51	2.31	5.3
C-F-40	3.22	4.09	

Fig. 39 shows the hysteretic curves for CFT columns of group C.

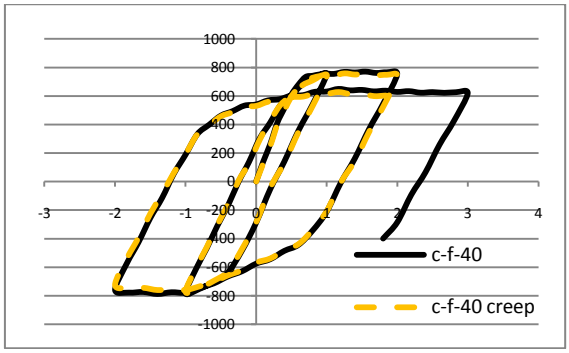

Figure 37.Hysteretic curves for CFT columns of group C

- GROUP D

Fig. 40 shows the hysteretic curves for CFT columns of group D. According to table 8, by increasing the yield stress, reduction percentages of sustainable shear force decrease in the same drifts. Creep causes a reduction in ductility ratio of specimens. These decreases for specimens D-fy-2, D-fy-3, D-fy-4 are 6.7%, 5.4% and 1.16%, respectively.

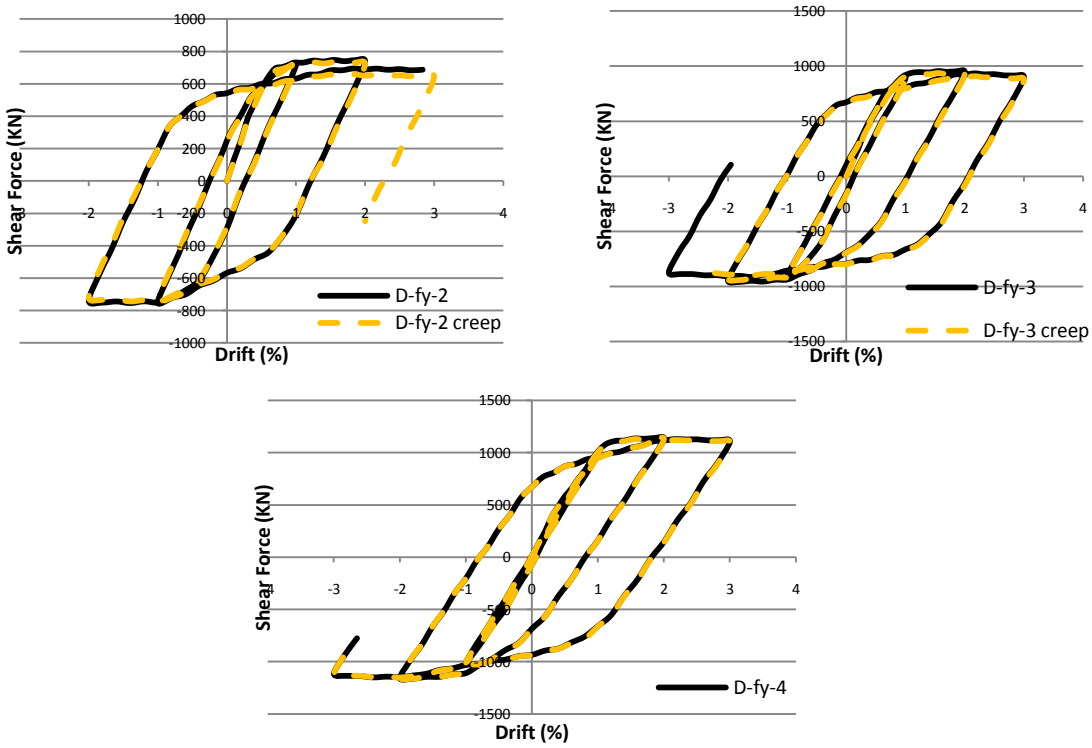

Figure 38. Hysteretic curves for CFT columns of group D

Also as an average amount, creep causes a reduction of 1.66% in energy absorption capacity of CFT columns.

Table 8: Reduction percentages of sustainable shear force for specimens of group D according to Fig. 40

Specimen	Drift		
	1%	2%	3%
D-fy-2	1.51	2.31	5.3
D-fy-3	1.12	1.93	2.5
D-fy-4	1.02	1.33	1.62

- GROUP E

Fig. 41 shows the hysteretic curves for CFT columns of group E. According to Table 9, by increasing the slenderness of CFT columns, reduction percentages of sustainable shear force increase in the same drifts. Creep causes a reduction in ductility ratio of specimens. These decreases for specimens E-S-3, E-S-5, E-S-8 are 1.8%, 7% and 8.22%, respectively. Also as an average amount, creep causes a reduction of 2.3% in energy absorption capacity of CFT columns.

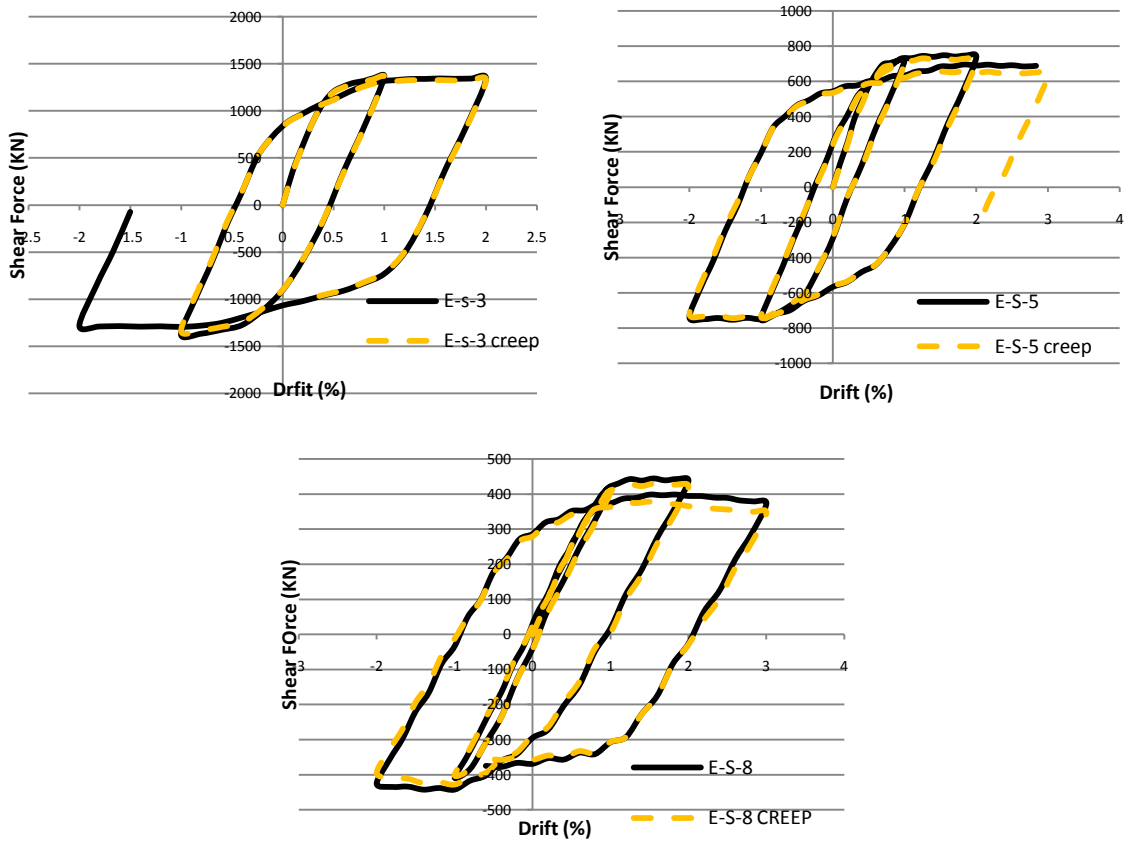

Figure. 41 Hysteretic curves for CFT columns of group E

Table 9: Reduction percentages of sustainable shear force for specimens of group E according to Fig. 41

Specimen	Drift		
	1%	2%	3%
E-S-3	0.72	1.21	-------
E-S-5	1.51	2.31	5.3
E-S-8	2.29	3.6	6.88

7. CONCLUSION

In the present study, at first, the effects of long-term axial loads (1 year) which are less than 40% of axial capacity of the CFT columns, have been studied. As an average amount, creep causes almost 40% reduction in Von-Mises stress at concrete nodes and almost 30% increase in Von-Mises stress at steel nodes near the region of supports. The stress increase in steel tube may be large enough to cause local buckling of the steel. Also the amount of axial creep is not affected by the length of specimen. Then, at the second step, by applying lateral displacements, the effect of cyclic loading on the creeped CFT column has been investigated. Based on the results, creep causes reduction of sustainable shear force in each cycle in the same drifts. The reduction percentages increases by increasing the amount of axial load and lateral displacement and varies between 0.72-6.88% in all groups. Also, as an average value for all of the groups, creep causes a reduction of almost 7% in ductility ratio of CFT specimens. Finally, creep causes a reduction in energy absorption capacity. The reduction percentage increases by increasing lateral displacement and is between 0.46 - 4.12%., and as an average amount is almost 2%. Finally, among all of the specimens, creep has significant effects on selender specimen and it has to consider in selender column's design.

REFERENCES

1. Furlong RW. Strength of steel-ecased concrete beam columns, *Journal of the Structural Division*, No. 5, **93**(1967) 113-24.
2. Terrey PJ, Bradford MA, Gilbert RI. Creep and shrinkage in concrete-filled steel tubes, *International Symposium on Tubular Structures*, Melbourne, 1994.
3. Morino S, Kawaguchi J, Cao ZS. Creep behavior of concrete-filled steel tubular members, *Proceeding Engineering Foundation conference on Composite Construction in Steel and Concrete*, Irsee, Germany, ASCE, 1997, pp. 514-25.
4. Ichinose LH, Watanabe E, Nakai H. An experimental study on creep of concrete filled steel pipes, *Constructional Steel Research*, **57**(2001) 453-66.
5. Peng JX, Shao XD, Cheng XY, Huang ZY. Creep behavior of concrete-filled steel tubular arch rib, *Engineering Mechanics*, No. 6, **24**(2007) 79-85.
6. Wang YF, Han B. Creep analysis of axially compressed concrete filled steel tube members, *EPMESC VII*, in EA Oliveira (ed.), Elsevier Press, Macao, (1999) 268-79.

7. Wang YF, Han B. Creep analysis of axially compressed concrete filled steel tubular members, *China Journal of Highway and Transport*, No. 2, **13**(2000) 57-60.
8. Naguib W, Mirmiran A. Creep modeling for concrete-filled steel tubes, *Constructional Steel Research*, **59**(2003) 1327-44.
9. Wang YF, Lei Y, Han B. Creep analysis of axially compressed high-strength concrete filled steel tubular columns, *ASCCS 06*, 2006.
10. Kwon SH, Kim TH, Kim YY, Kim JK. Long-term behaviour of square concrete-filled steel tubular columns under axial service loads, *Magazine of Concrete Research*, No. 1, **59**(2007) 53-68.
11. Han B, Wang YF. Long-term load carrying capacity of axially compressed concrete filled steel tubular short columns, *ISCC 2004*, South California University Press, Changsha, 2004.
12. Prion H, Boehme J. Beam-column behavior of steel tubes filled with high strength concrete, *Canadian Journal of Civil Engineering*, No. 2, **21**(1994) 207-18.
13. Boyd P, Cofer WF, McLean DE. Seismic performance of steel-encased concrete columns under flexural loading, *ACI Structural Journal*, No. 3, **92**(1995) 355-64.
14. Alfawakiri F. Behavior of high strength concrete-filled circular steel tube beam columns, MS thesis, University of Ottawa, Ottawa, 1997.
15. Help, *ANSYS 12.0*, 2010.
16. Help, *ANSYS Civil FEM 12.0*, Ingesiber, 2010.
17. Wang YF, Han B, Zhang DJ. Advances in creep of concrete filled steel tube members and structures, *Proceedings of the Concreep8 Conference*, Taylor & Francis, Ise-Shima, Japan, 2009.
18. Gopalakrishnan KS, Neville AM, Ghali A. Creep Poisson's ratio of concrete under multi-axial compression, *ACI Journal Proceedings*, American Concrete Institute, No. 12, **66**(1969) 1008-20.
19. Illston JM, Jordan IJ. Creep prediction of concrete under multiaxial stress, *ACI Journal Proceedings*, American Concrete Institute, No. 14, **69**(1972) 158-64.
20. Choi SM, Kang SB, Kim DJ. Hysteresis performance of CFT columns subjected to low axial force and cyclic lateral loads, *Journal of Korean Society of Steel Construction (KSSC)*, **15**(2003) 207-17.
21. Abedi K, Ferdousi A, Afshin H. A novel steel section for concrete-filled tubular columns, *Thin-Walled Structures*, **46**(2008) 310-19.